An encoding model of temporal processing in human visual cortex

Anthony Stigliani[1], Brianna Jeska[1], & Kalanit Grill-Spector[1,2]

[1] Department of Psychology, Stanford University, Stanford, CA 94305, USA

[2] Stanford Neurosciences Institute, Stanford University, Stanford, CA 94305, USA

ABSTRACT

How is temporal information processed in human visual cortex? Visual input is relayed to V1 through segregated transient and sustained channels in the retina and LGN. However, there is intense debate as to how transient and sustained channels contribute to visual processing beyond V1. Using a 2 temporal-channel encoding model we can predict fMRI responses to time-varying stimuli ranging from milliseconds to seconds. The transient channel dominates responses in the periphery of early visual cortex and lateral occipito-temporal regions. However, both sustained and transient channels drive responses in central early visual cortex and ventral occipito-temporal regions. Together these finding resolve an outstanding debate and lay the foundation for a complete temporal model of neural processing in visual cortex. Importantly, this encoding approach can be applied with fMRI to decipher neural computations in millisecond resolution in any part of the brain, which has vast implications for understanding neural processing.

Keywords: BOLD, fMRI, V1, V4, MT, extrastriate cortex, temporal channels, transient, sustained

How does the visual system process the temporal aspects of the visual input? In the retina[1] and LGN[2-4] temporal processing is thought to be mediated predominately by a magnocellular (M) pathway distinguished by its large transient responses[3, 4] and a parvocelluar (P) pathway which has larger sustained responses than the M pathway[3, 4] (in addition to a smaller koniocelluar[5] pathway). While M and P pathways remain segregated up to striate cortex (V1), there is intense debate as to how these pathways contribute to visual processing in extrastriate cortex. The prevailing view suggests that the dorsal stream, particularly MT, is M dominated[6-8], and the ventral stream, particularly V4, is P dominated[9-11]. However, an opposing view suggests that these pathways are not segregated in extrastriate cortex[5, 8] as there are substantial M and P contributions to both V4[5, 9] and MT[12, 13].

As M and P pathways are associated with transient and sustained responses, respectively, these theories make predictions regarding temporal processing in human visual cortex. The prevailing view predicts that hMT+ will have large transient but small sustained responses, and conversely hV4 will have large sustained but small transient responses. However, the opposing view predicts substantial transient and sustained responses in both hMT+ and hV4. While these predictions are derived from studies of the macaque brain, the human visual cortex contains additional regions. E.g., on the ventral cortical surface, hV4 is neighbored by areas VO-1 and VO-2[14], and on the lateral surface, hMT+ is neighbored by LO-1 and LO-2[15]. Therefore, generating a complete model of temporal processing in human visual cortex necessitates measurements in humans.

Except for a few studies[16, 17], understanding temporal processing in human visual cortex has seen little progress for two main reasons. First, the temporal resolution of fMRI is in the order

of seconds[18], an order of magnitude longer than the timescale of neural processing, which is in the tens to hundreds of milliseconds[17] range. Second, while fMRI responses are largely linear for long stimulus presentations[19, 20], they exhibit marked nonlinearities for short or transient stimuli[19-24]. Since the standard linear model for fMRI[19, 25] is inadequate for modeling responses to such stimuli and fMRI is slow, the temporal processing characteristics of human visual cortex remain elusive.

If the observed nonlinearities are of neural (rather than BOLD) origin, a new encoding approach[26-29], which uses computational models to predict neural responses, could surmount these issues. Different than the standard model, which directly relates the stimulus to fMRI signals via convolution with a hemodynamic response function (HRF), the encoding approach first models neural responses to the stimulus; these neural responses are convolved with the HRF to yield fMRI signals. The encoding approach has been influential for two reasons: (i) it provided an important insight that accurately modeling neural responses at a sub-voxel resolution better predicts fMRI responses at the voxel resolution, and (ii) it advanced understanding of neural mechanisms by building explicit quantitative models of neural computations.

Here we sought to leverage the encoding approach to characterize temporal processing in human visual cortex. Thus, we built a temporal encoding model of neural responses to time-varying visual stimuli in millisecond resolution and used this model to predict fMRI responses in second resolution. The model is based on estimation of the transient and sustained channels' impulse response functions from measurements in macaque V1[30-32] and psychophysics in humans[33-35]. To determine temporal processing in visual cortex we devised three experiments aimed to measure fMRI responses to time-varying visual stimuli that were either sustained (1

continuous image per trial, durations ranging from 2 s to 30 s; **Fig. 1**, *Experiment 1*), transient (30 flashed, 33 ms long, images per trial, inter-stimulus intervals ranging from 33–967 ms; **Fig. 1**, *Experiment 2*), or contained both transient and sustained components (30 continuous images per trial, durations ranging from 67–1000 ms per image; **Fig. 1**, *Experiment 3*)*. We asked: (i) Do millisecond temporal variations in visual stimuli generate reproducible modulations of fMRI responses in visual cortex? (ii) Does a 2 temporal-channel encoding model predict fMRI responses to stimuli that vary in their temporal properties from milliseconds to seconds? (iii) How do sustained and transient channels contribute to neural responses in striate and extrastriate cortex?

RESULTS

Do Millisecond Temporal Variations in the Visual Stimulus Modulate V1 Responses?

To test the feasibility of this approach, we first examined V1 responses during the three experiments. Since predicted fMRI responses from the standard model depend only on the duration of stimuli, the standard model predicts longer responses for longer trials and identical responses in Experiments 1 and 3 (**Fig. 2a**, *blue and green*), which use the same visual stimuli and trial durations and just vary by the number of images per trial (1 vs. 30, respectively). Furthermore, the model predicts that the amplitude of responses in Experiments 1 and 3 will increase from 2–8 s trials and will remain largely the same for longer trials. While the standard model predicts the same response durations in Experiment 2, it predicts substantially lower response amplitudes in Experiment 2 than Experiments 1 and 3 because the transient visual stimuli are presented for only a fraction of each trial. Furthermore, the model predicts a

progressive decrease in response amplitude during Experiment 2 from 2–30 s trials as the fraction of the trial in which visual stimuli are presented decreases (from 1/2 to 1/30 of the trial, **Fig. 2a**, *red*).

While V1 responses to sustained visual stimulation in Experiment 1 largely followed the predictions of the standard model (**Fig. 2a**, *blue*), responses in Experiments 2 and 3 deviated from the standard model's predictions. First, responses in Experiment 3 (**Fig. 2b**, *green*) were higher than responses in Experiment 1 for all trial durations. Second, responses to transient stimuli in Experiment 2 (**Fig. 2b**, *red*) were substantially higher than predicted by the standard model. In fact, V1 responses during 2–8 s trials of Experiment 2 were equal or higher than those of Experiment 1, even though the cumulative duration of stimulation across images in Experiment 2 was a fraction of the duration of stimulation in Experiment 1. Third, different than the predictions of the standard model, response amplitudes in Experiment 2 did not systematically decline with trial duration but instead peaked for the 4 s trials.

These data demonstrate that (i) varying the temporal characteristics of visual presentation in the millisecond range has profound effects on V1 fMRI responses, and (ii) the standard model is inadequate in predicting measured fMRI responses for these stimuli, in agreement with prior data. Furthermore, the higher responses in Experiment 3 (which has both sustained and transient visual stimulation) compared to Experiments 1 and 2 (which have either sustained or transient stimuli, respectively) suggest that both transient and sustained components of the visual input contribute to the fMRI signals, consistent with our hypothesis.

An Encoding Model for Temporal Processing in Visual Cortex

To accurately predict fMRI responses in all three experiments, we built a temporal encoding model of neural responses in millisecond resolution and used this model to predict fMRI responses in second resolution (**Fig. 3**). Our model consists of 2 neural temporal channels, each of which can be characterized by a linear systems approach using a temporal impulse response function[17, 30-32, 34, 35] (IRF). The sustained channel is characterized by a monophasic IRF (**Fig. 3b**, *blue channel IRF*) peaking at around 40 ms and lasting 100–150 ms; convolving this channel with a visual stimulus will produce a sustained neural response for the duration of the stimulus. The transient channel is characterized by a biphasic IRF, akin to a derivative function, with the positive part peaking at around 35 ms and the negative part peaking at around 70 ms (**Fig. 3b**, *red channel IRF*). A squaring nonlinearity is added, as both stimulus onset and offset lead to increased neural firing and consequently increased metabolic demands[17, 36]. Thus, convolving the visual stimulus with this transient IRF will produce a positive neural response when there is an onset or offset of the visual stimulus but zero response in between when the stimulus is presented for durations longer than the duration of the IRF. The predicted fMRI response is generated by convolving the output of each neural channel with the HRF and summing the responses of the two temporal channels (**Fig. 3c**).

Our procedure for testing the 2 temporal-channel encoding model had two stages. First, we estimated the contributions of the two temporal channels to fMRI signals using concatenated data from Experiments 1 and 2 that were designed to largely drive sustained or transient channels, respectively. Second, we cross-validated the model by testing how well it predicted data from a third experiment that had both transient and sustained visual stimulation. As a

benchmark, we compared the performance of the 2 temporal-channel model with the standard model.

Does a 2 Temporal-Channel Model Explain V1 fMRI Responses to Time-Varying Stimuli?

Comparing the predictions of the 2 temporal-channel model to V1 responses reveals three findings. First, the 2 temporal-channel model containing one sustained predictor (weighted by β_S) and one transient predictor (weighted by β_T) generated fMRI signals that tracked both the duration and amplitude of V1 responses in Experiments 1 and 2 (**Fig. 4a**, compare model prediction, *black*, to measured V1 data, *gray*). Consistent with our predictions, the sustained channel accounted for the majority of responses in Experiment 1 (**Fig. 4a**, *top row*, *blue*), while the transient channel contributed the bulk of the response in Experiment 2 (**Fig. 4a**, *bottom row*, *red*).

Second, the 2 temporal-channel model explains V1 responses to both Experiments 1 and 2, but the standard model fails to explain responses to transient stimuli in Experiment 2. That is, the 2 temporal-channel model fit to both experiments, explained 62% ± 3% (mean ± 1 standard error of the mean across participants, SEM) of V1 response variance in Experiment 1 (**Fig. 4d**) and 51% ± 3% of the variance in Experiment 2 (**Fig. 4e**). In contrast, the standard model fit to both experiments explained 61% ± 3% of the variance in Experiment 1 (**Fig. 4d**) but less than 1% ± 1% of the variance in Experiment 2 (**Fig. 4e**). Thus, while the standard model captured V1 responses to the long stimulus presentations in the first experiment, it failed to capture responses to transient stimuli in the second experiment.

Third, the 2 temporal-channel model with β_S and β_T fit from Experiments 1 and 2 (**Fig. 4c**) accurately predicted independent data from Experiment 3 (**Fig. 4b**). The sustained contribution (**Fig. 4a-b**, *blue*) in Experiment 3 was comparable to Experiment 1 (these experiments have the same total duration of stimulation per trial), and the transient contribution (**Fig. 4a-b**, *red*) in Experiment 3 was similar to Experiment 2 (these experiments have the same number of transients per trial). Since both temporal channels provided a significant contribution to V1 and the contributions of the two channels are additive, Experiment 3 responses were higher than both Experiments 1 and 2 across all trial durations. Analysis of cross-validated R^2 showed that the 2 temporal-channel model explained 71% ± 2% of variance in Experiment 3 (**Fig. 4f**) even though the channel weights were estimated from responses to independent data with different temporal characteristics. The cross-validated R^2 of the 2 temporal-channel model was also significantly higher than the standard model (t_{11} = 5.92, p < 0.001, paired t-test), which only explained 63% ± 3% of response variance in Experiment 3 (**Fig. 4f**). Thus, the 2 temporal-channel model predicts V1 fMRI responses to visual stimuli across a three-fold range of presentation durations ranging from tens of milliseconds to tens of seconds.

Do Temporal Processing Characteristics Differ Across Intermediate Visual Areas?

We next examined hV4 and hMT+ responses to the time-varying visual stimuli in Experiments 1–3, as the competing theories make different predictions regarding the contributions of sustained and transient channels to these regions. hV4 and hMT+ illustrated distinct patterns of responses. Like V1, hV4 showed higher responses in Experiment 3 (30 continuous images per trial) than either Experiment 1 (1 continuous image per trial) or

Experiment 2 (30 flashed images per trial). Different from V1, hV4 exhibited equal or stronger responses to the brief transient visual stimuli in Experiment 2 than the sustained single images in Experiment 1 (**Fig. 5a**). Different than both V1 and hV4, hMT+ exhibited close to zero evoked responses for the sustained stimuli in Experiment 1 (except for onset and offset responses that are visible in trials of 8 s and longer, **Fig. 5b**). However, hMT+ showed substantial responses for transient stimuli in Experiment 2 that were comparable to Experiment 3, which had both transient and sustained stimulation. Together, these data suggest differences in temporal processing across hV4 and hMT+.

Next, we quantified hV4 and hMT+ responses with the 2 temporal-channel encoding model. The model fits revealed that (i) in hV4 both channels contributed to responses, with the contribution of the transient channel about double that of the sustained channel (**Fig. 5a**, *inset*) and (ii) in hMT+ the transient channel substantially contributed to responses, but the sustained channel had close to zero contribution (**Fig. 5b**, *inset*). Across both regions, the 2 temporal-channel model fit data from Experiment 2 better than the standard model (ts > 4.06, ps < 0.01, paired t-test on R^2 values for each ROI), and also better predicted data from Experiment 3 than the standard model (ts > 4.18, ps < 0.05, paired t-test on cross-validated R^2 values for each ROI; **Fig. 5c**). These results demonstrate that not only does the 2 temporal-channel model perform significantly better than the standard model at intermediate stages of the visual hierarchy, but that the contributions of transient and sustained channels differ across hV4 and hMT+.

What is the Topology of Sustained and Transient Channels Across Visual Cortex?

To complement the ROI approach, we next visualized the spatial topology of the sustained and transient channels across visual cortex, which enables mapping channel contributions at the voxel-level.

Examining the contribution of sustained and transient channels across ventral and lateral occipito-temporal cortex revealed two main findings. First, lateral occipito-temporal cortex was devoid of contributions from the sustained channel, but had substantial contributions from the transient channel (**Fig. 6a**). This effect was widespread and included not only voxels in hMT+, as predicted by the prior analysis, but also extended (i) posteriorly into portions of lateral occipital areas LO-1 and LO-2, and (ii) ventrally into the inferior occipital gyrus and lateral fusiform gyrus. Dorsal regions along the intraparietal sulcus also showed negligible sustained responses (**Supplementary Fig. S3b**). Second, in ventral occipito-temporal cortex, regions along the posterior collateral sulcus and medial fusiform gyrus (where hV4, VO-1, and VO-2 are located) showed both transient and sustained responses, with larger contributions from the transient than sustained channel (**Fig. 6a**).

We quantified the mean contributions of transient and sustained channels across visual areas spanning occipito-temporal cortex. Our results showed differences in the contributions of sustained and transient channels across early visual cortex (V1–V3), ventral occipito-temporal cortex (hV4 and VO-1/2), and lateral occipito-temporal cortex (LO-1/2 and hMT+, **Fig. 6b**, significant temporal-channel by cluster interaction, $F_{2,\,22} = 13.16$, $p < 0.001$, two-way ANOVA on β weights with factors of temporal-channel [sustained/transient] and visual cluster [early/ventral/lateral]). From V1 to higher-order areas, there was a larger drop in the

contribution of the sustained channel than the transient channel (**Fig. 6b**). Nevertheless, there were significant differences among clusters, whereby in ventral areas both sustained and transient channels contributed to responses, but in lateral areas responses were dominated by the transient channel.

The spatial topology of sustained and transient channels also revealed differences in temporal processing within regions. Specifically, in early visual cortex (V1–V3) the sustained channel was robust in eccentricities < 20°, but declined in more peripheral eccentricities (**Fig. 7a**, *right*). In contrast, the transient channel contributed to responses across all eccentricities including peripheral ones (> 20°; **Fig. 7a**, *left*). We quantified these effects by measuring the contributions of the 2 temporal-channels across eccentricities using uniformly-sized disc ROIs defined along the horizontal meridian representations in V1 and V2/V3 (**Fig. 7b**). This quantification showed that in early visual areas the magnitude of the sustained channel declined more rapidly with eccentricity than the transient channel, to the extent that at eccentricities of 40° there still was a 0.90 ± 0.17% transient response but less than 0.26 ± 0.07% of a sustained response (**Fig. 7b**). Further, the decline of the sustained channel with eccentricity occured more rapidly in V2/V3 than V1. Together, we find a differential contribution of transient and sustained channels across eccentricities and areas (significant three-way interaction of temporal channel [sustained or transient], visual area [V1 or V2/V3], and eccentricity [5°, 10°, 20°, or 40°], $F_{3, 33}$ = 3.18, $p < 0.05$, three-way ANOVA on the β weights).

DISCUSSION

Our results show that a 2 temporal-channel model of neural responses, containing sustained and transient channels, is a parsimonious encoding model that predicts fMRI responses in human visual cortex to visual stimuli across a broad range of durations spanning from tens of milliseconds to tens of seconds. The transient channel dominates responses in lateral occipito-temporal regions and peripheral eccentricity representations of early visual cortex. However, both sustained and transient channels drive responses in ventral occipito-temporal regions as well as foveal and parafoveal eccentricities of early visual cortex. Critically, our data address the ongoing debate regarding the contribution of sustained and transient channels in extrastriate cortex. Consistent with the prevailing view[2, 6, 7], we find that the transient channel dominates hMT+ responses and show for the first time that this characteristic extends to human lateral occipito-temporal cortex more generally. In contrast, we find a surprisingly large transient contribution to responses in hV4 and neighboring ventral occipito-temporal regions, suggesting that not just sustained but also transient channels drive responses in ventral extrastriate cortex.

Differential Transient and Sustained Responses Across Visual Cortex

Our research fills a large gap in knowledge regarding temporal processing in human visual cortex by showing that (i) the 2 temporal-channel model is applicable to at least 10 additional visuals areas beyond V1[17, 30-32], and (ii) temporal processing is a key functional attribute that differentiates visual areas.

Our observation that hMT+ responses to sustained stimuli are close to zero is consistent with the prevailing view that (i) hMT+ is involved in processing visual dynamics rather than static

information, and that (ii) inputs to hMT+ are M dominated[7]. Notably, we found that neighboring regions, LO-1 and LO-2, also have close to zero sustained responses. This finding is interesting because LO-2, which is thought to be involved in visual processing of objects[15, 37] and bodyparts[38], shows more robust responses to rapidly presented stimuli compared to nearby category-selective regions[39]. The present data suggest that this characteristic may be an outcome of a dominant transient channel – a hypothesis that can be tested in future research.

Inconsistent with the prevailing view, we found that hV4 showed not only sustained responses as expected[8, 10, 24, 40], but also large transient responses. This observation is consistent with findings of both P and M inputs to V4[5, 9]. While the sustained channel has been associated with coding static visual input and the transient channel with coding visual dynamics[10, 11, 41], transient visual information is also indicative of changes to the content of the visual scene. Indeed, in our experiments, transients occurred when the content of stimuli changed (i.e., when a new image was shown or an image was replaced by a uniform gray screen). Since the function of the ventral stream is to infer what is in the visual scene, it is beneficial for ventral regions to be sensitive to changes in the visual input[42]. Results of our experiments suggest that ventral stream regions (hV4, VO1/2) are in fact sensitive to rapid changes to the visual scene. Transient processing in the ventral stream may foster detection of novel stimuli and rapid extraction of the gist of the visual input.

It is interesting that temporal processing in lateral occipito-temporal regions, like that of far peripheral eccentricities (> 20°) in early visual cortex, was dominated by the transient channel, and temporal processing in ventral occipito-temporal regions, like lower eccentricities in early visual cortex, showed a dual channel contribution. These functional characteristics may be

anatomically supported by white matter connections from peripheral representations of early visual areas to MT and nearby regions[43] and white matter connections from central representations of early visual cortex to ventral occipito-temporal regions[44]. Furthermore, the diminished sustained responses in the periphery of early visual cortex is consistent with prior findings showing reduced P inputs[45] and diminished sustained luminance responses[17] in peripheral compared to central V1, as well as faster perception in the periphery[46].

Implications for Modeling fMRI Signals: Millisecond Timing Matters

Our data have important implications regarding modeling fMRI signals and interpreting results of temporal processing in the human brain because they show that (i) varying the temporal characteristics of the visual stimulus in the millisecond range has observable effects on fMRI responses in the second range and (ii) by considering the contribution of a transient neural channel, the encoding model can account for nonlinearities in fMRI responses for rapid and short visual stimuli[19-21, 23, 47].

Our data extend the original linear model of fMRI signals[19, 25] by showing the importance of modeling the temporal properties of neural responses at millisecond resolution to accurately predict fMRI signals. In their original study, Boynton et al.[19] noted consistent deviations from the linear (standard) model in short durations (3–6 s) in which the model underestimated fMRI signals. These nonlinearities are exacerbated in experiments using even shorter stimuli (1/4 to 2 s[21, 23, 47]). Boynton and colleagues suggested that neural adaptation or transient responses may explain deviations from linearity. We favor the interpretation that transient responses account for nonlinearities for two reasons: (i) Taking into account the neural transient channel resolves

this nonlinearity and can predict not only our measurements but also prior data showing nonlinearities[23] (**Supplementary Fig. S4**). (ii) Adaptation would have resulted in declining responses during long trials of continuous presentation of a single stimulus[42]. However, we observed negligible adaptation in early (e.g. V1) and intermediate (e.g. hV4) areas even during the 30 s single continuous image trials. As adaptation increases across the visual hierarchy[40, 48], adding to the 2 temporal-channel model an adaptation component[20] or compressive temporal summation[49] may enhance model fits in higher-order areas.

It is worthwhile noting that while the 2 temporal-channel model provides a significant improvement in modeling fMRI signals, our model does not explain the entire variance of fMRI signals (**Supplementary Fig. S2**). Therefore, an important direction for future research will be to combine the 2 temporal-channel model with a spatial receptive field model[26-29] to generate a complete spatio-temporal understanding of visual responses.

Given the pervasive use of the standard linear model in fMRI research, our results have broad implications for fMRI studies in any part of the brain. We find that timing of stimuli in the millisecond range has a large impact on the magnitude of fMRI responses, which has important implications for interpreting results of studies that vary the temporal characteristics of stimuli across conditions (e.g.[50]). Critically, we demonstrate that rather than ignoring fast cortical processing because of nonlinearities in the standard model, it is possible to generate neural predictions at sub-second resolution and use them to accurately predict fMRI responses. This encoding approach thus opens exciting new opportunities for investigating fast cortical mechanisms using fMRI in many domains including somatosensory, auditory, and high-level cognitive processing.

In sum, our experiments elucidate the characteristics of temporal processing across human visual cortex. These findings are important because they (i) explicate for the first time the contribution of transient and sustained visual responses across human visual cortex beyond V1, and (ii) show that accounting for neural responses at the millisecond range has important consequences for understanding fMRI signals in the second range in any part of the brain.
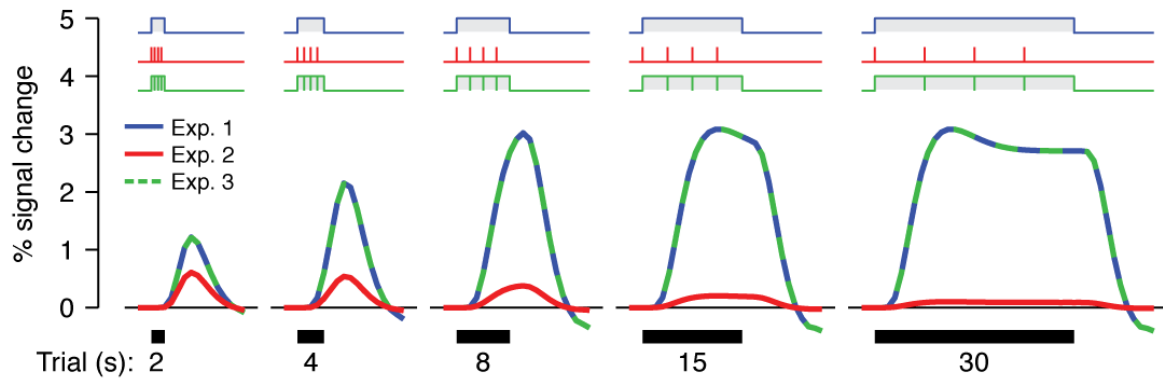
ACKNOWLEDGEMENTS
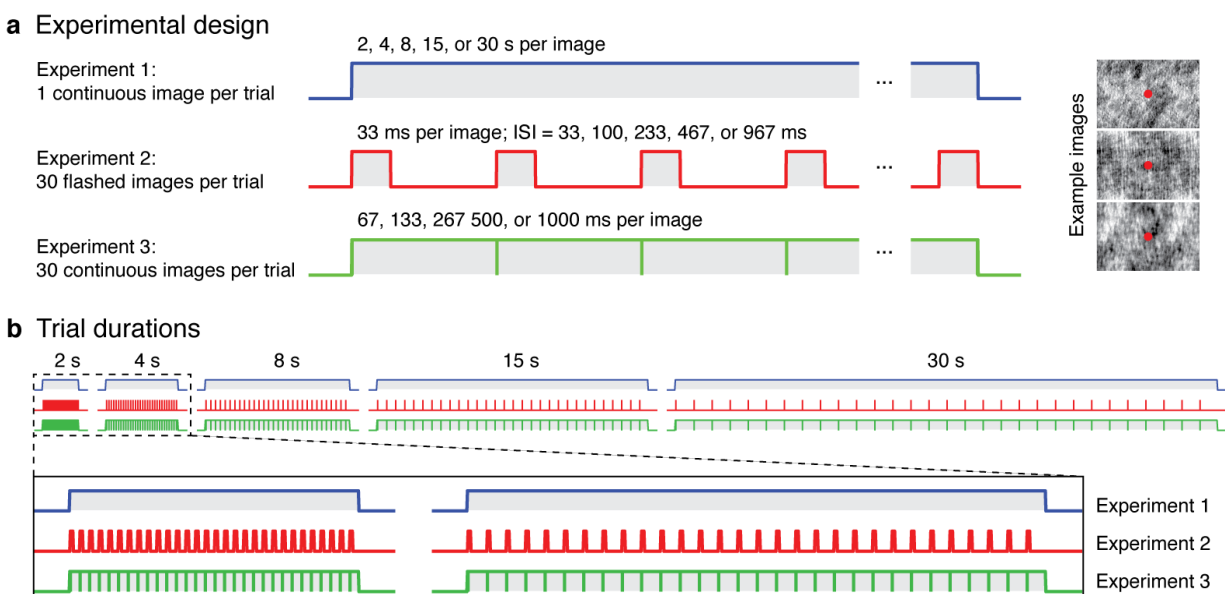
FIGURES

Figure 1: Measuring brain responses to combinations of sustained and transient visual stimuli: Experimental design. (**a**) Participants fixated centrally and viewed phase-scrambled gray-level images that were presented in trials of different durations, interleaved with 12 s periods of a blank screen. The same fixation task (detecting change in fixation color) was used in all three experiments. *Experiment 1:* a single phase scrambled image was shown for the duration of a trial. *Experiment 2:* 30 briefly presented images (33 ms each), each followed by a blank screen, were presented in each trial. As the trial duration lengthens, the gap between images increases, causing the fraction of the trial containing visual stimulation to decrease. *Experiment 3:* 30 continuous images (with no gaps between consecutive stimuli) were presented in each trial. As the block duration lengthens, the duration of each image progressively increases. (**b**) The same trial durations (2, 4, 8, 15 or 30 s) were utilized across all three experiments while the rate and duration of visual presentation varied between experiments. Corresponding trials in Experiments 1 and 3 have the same overall duration of stimulation but different numbers of stimuli, whereas trials in Experiments 2 and 3 have the same number of stimuli but different durations of stimulation. *Top:* stimulation durations for example trial in each experiment; *Bottom:* zoom on the 2 s and 4 s trials.
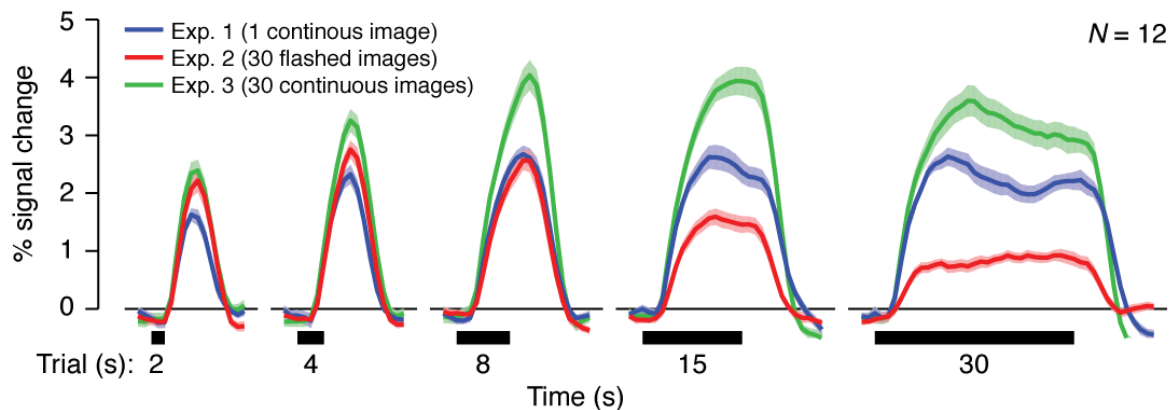
Figure 2: V1 responses to transient stimuli differ from the predictions of the standard model.
(**a**) The standard model predicts the same response in trials of the same duration across Experiment 1 (*blue*) and Experiment 3 (*green*), since both present stimuli continuously for the same total duration in each trial. However, responses in Experiment 2 (*red*) are predicted to be much lower because stimuli are spaced apart and are only presented for a fraction of each trial duration. (**b**) The mean V1 response in Experiments 1–3 averaged across 12 participants. Each curve is data from a different experiment (see legend). Shaded regions around the curves indicate ± 1 standard error of the mean (SEM) across 12 participants. In both (a) and (b) the onsets and lengths of the trials are illustrated as thick black bars below each graph, and curves extend 2 s before the onset and 12 s after the offset each trial.
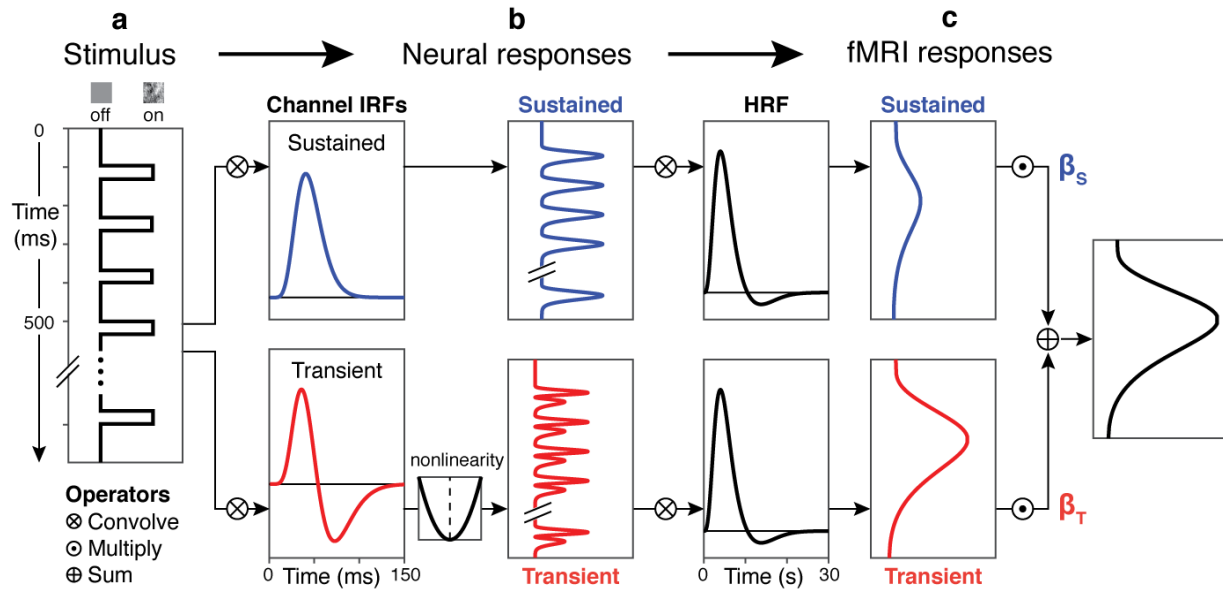
Figure 3: The 2 temporal-channel model. (**a**) Transitions between stimulus and baseline screens are coded as a step function representing when a stimulus was on vs. off with millisecond temporal resolution. In the example illustrated here, each stimulus is presented for 33 ms and followed by a 100 ms blank screen. (**b**) Separate neural responses for the sustained (*blue*) and transient (*red*) channels are modeled by convolving the stimulus vector with impulse response functions (IRFs) for the sustained and transient channels, respectively, estimated from human psychophysics. A squaring nonlinearity is applied in the transient channel to rectify offset deflections (see Online Methods). (**c**) Sustained and transient fMRI response predictors are generated by convolving each channel's neural responses with the hemodynamic response function (HRF) and downsampling to match the temporal acquisition rate of fMRI data. The total fMRI response is the sum of the weighted sustained and transient fMRI predictors for each channel. To estimate the contributions (β weights) of the sustained (β_S) and transient (β_T) channels in V1, we fit the 2 temporal-channel model across data concatenated across Experiments 1 and 2.
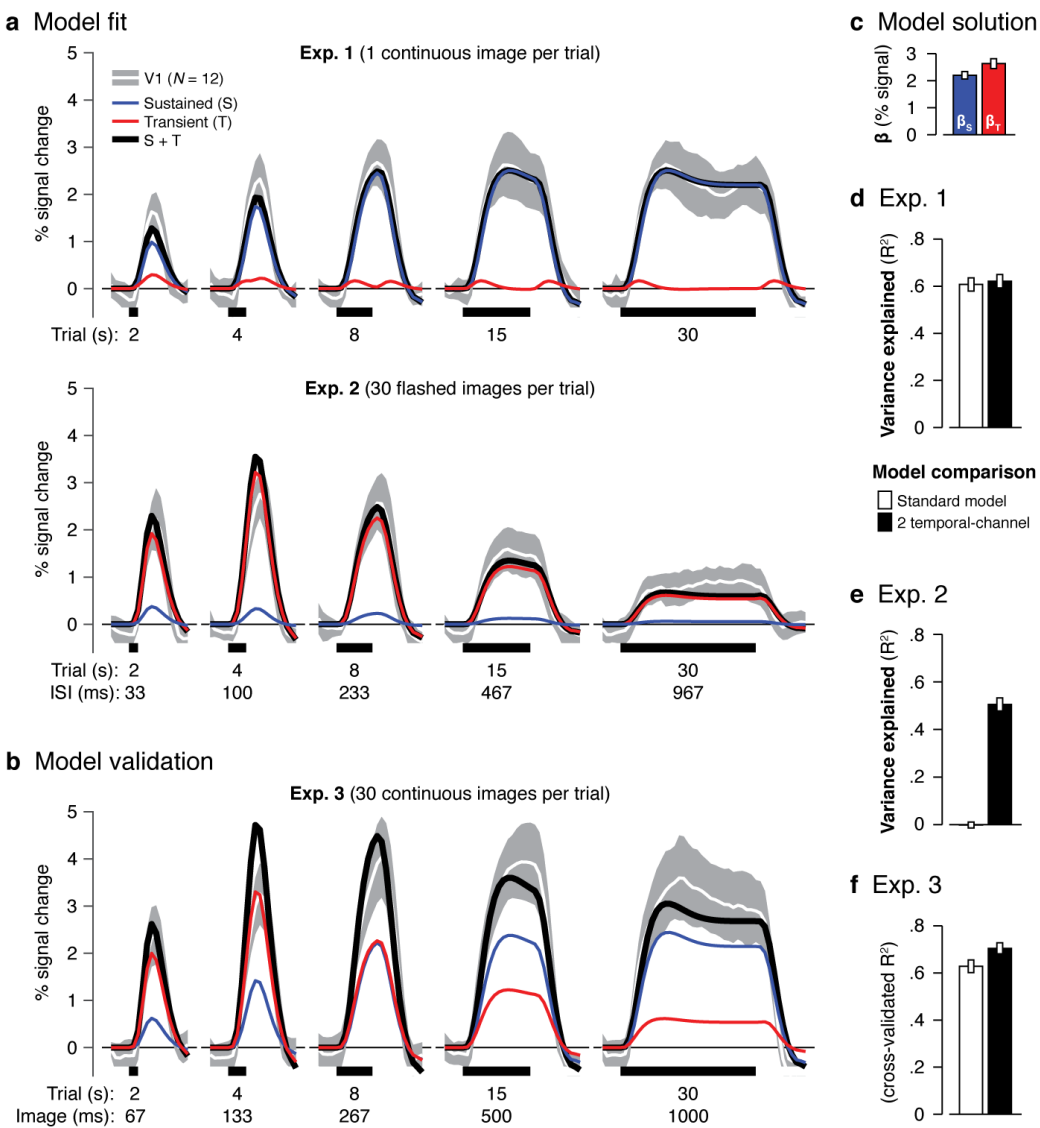
Figure 4: Sustained and transient contributions to V1 fMRI responses. (**a**) Measured V1 responses in Experiments 1 and 2 are plotted as the mean (*white*) ± 1 standard deviation (*gray*) across 12 participants for each trial duration. Superimposed are the predictions of the 2 temporal-channel model fit across data from both experiments. *Blue:* sustained predictor weighted by β_S; *Red:* transient predictor weighted by β_T; *Black:* prediction of the 2 temporal-channel model, which is the addition of the two channels. (**b**) Measured V1 responses and cross-validated model prediction for Experiment 3. The sustained and transient predictors are respectively weighted with β_S and β_T fitted from Experiments 1 and 2 [see (c)]. In all panels, trial durations are illustrated below the x-axis, and curves extend 2 s before the onset and 12 s after the offset each trial. (**c**) The model solution (β_S and β_T) for V1 fit with the two temporal-channel model using data concatenated across Experiments 1 and 2. (**d-f**) Comparison of the variance explained (R^2) by 2 temporal-channel model vs. the standard model for each experiment. Error bars in (c–f) indicate ± 1 SEM across participants.
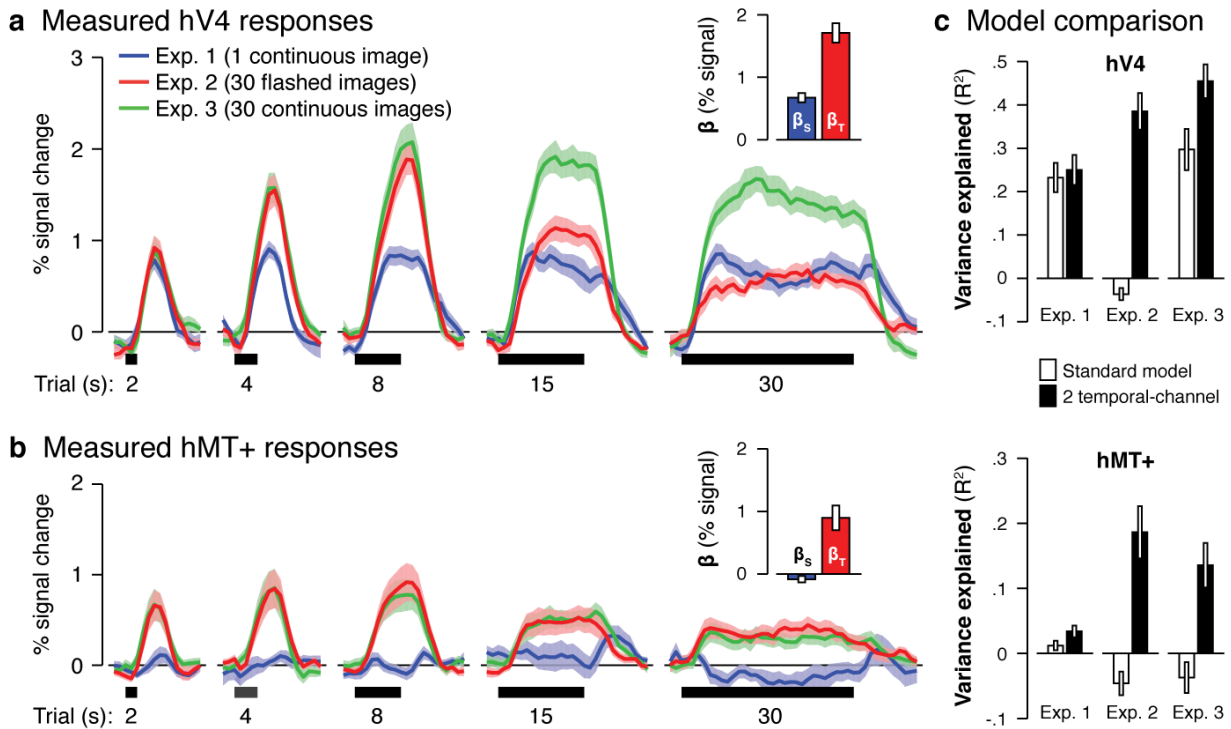
Figure 5: Differential sustained and transient contributions across hV4 and hMT+. (**a**) hV4 and (**b**) hMT+ responses for Experiment 1 (*blue*), Experiment 2 (*red*), and Experiment 3 (*green*). Curves show mean (solid line) ± 1 SEM across 12 participants (shaded area). Trial durations are indicated by the thick black lines below the x-axis, and curves extend 2 s before the onset and 12 s after the offset each trial. The model solution (β_S and β_T) for each region is plotted to as an inset with error bars representing ± 1 SEM across participants. (**c**) Comparison of the variance explained (R^2) by 2 temporal-channel model vs. the standard model, both fit across data from Experiments 1 and 2. Model performance is quantified separately for each experiment both for hV4 (*top*) and hMT+ (*bottom*). Error bars indicate ± 1 SEM across participants.
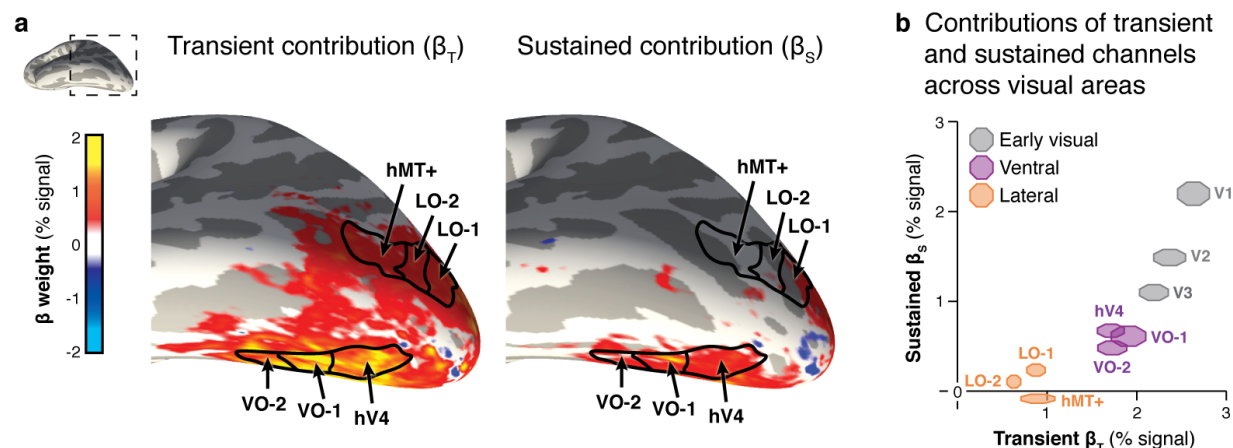
Figure 6: Differential transient and sustained contributions across ventral and lateral regions. (**a**) Ventrolateral view of occipito-temporal cortex (see inset) depicting group-averaged (*N* = 12) maps of the contributions of transient (*left*) and sustained (*right*) channels. We first estimated β weights of each channel in each voxel in each participant's native brain space. β weight maps were transformed to the FreeSurfer average brain using cortex-based alignment and averaged across participants in this common cortical space. The resulting group maps were thresholded to exclude voxels with weak contributions ($-0.1 > \beta > 0.1$). Boundaries of ventral and lateral regions (*black*) are derived from the Wang Atlas, with hMT+ as the union of TO-1 and TO-2. (**b**) Contributions (β weights) of transient (x-axis) and sustained (y-axis) channels to each visual area as estimated by the 2 temporal-channel model. Marker size spans ± 1 SEM across 12 participants in each dimension and β weights were solved by fitting the 2 temporal-channel using data concatenated across Experiments 1 and 2.
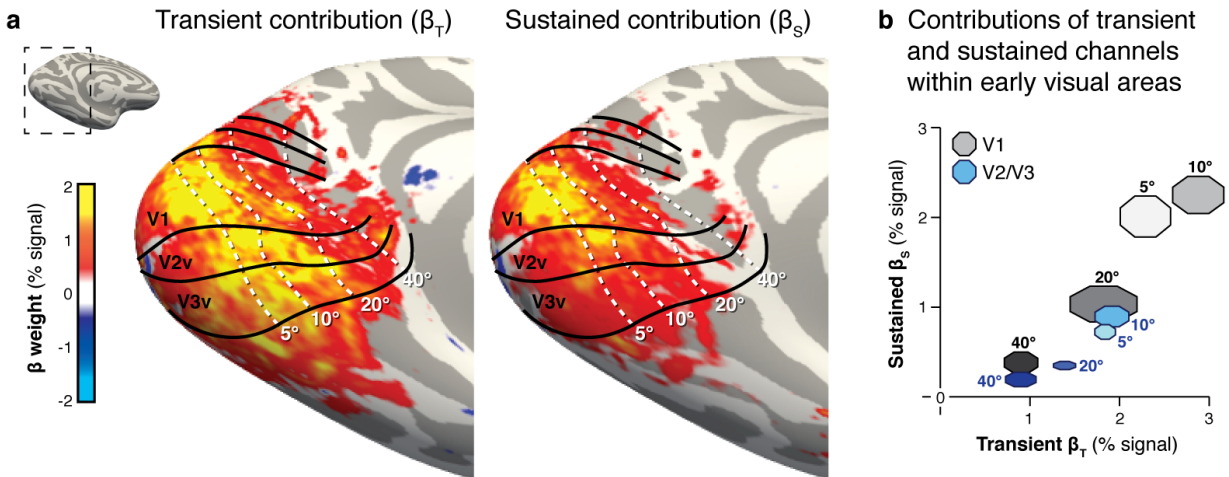
Figure 7: Differential transient and sustained contributions across central and peripheral eccentricities. (**a**) Medial cortical surface zoomed on the occipital lobe (see inset) depicting group-averaged (N = 12) maps of the contributions of transient (*left*) and sustained (*right*) channels. We first estimated β weights of each channel in each voxel in each participant's native brain space. β weight maps were transformed to the FreeSurfer average brain using cortex-based alignment and averaged across participants in this common cortical space. The resulting group maps were thresholded to exclude voxels with weak contributions ($-0.1 > \beta > 0.1$). Regional boundaries (*black*) and eccentricity bands (*white*) of early visual areas are derived from the Benson Atlas. (**b**) Contributions of transient (x-axis) and sustained (y-axis) channels across eccentricities along the horizontal representation in V1 (grays) and V2/V3 (blues) as estimated by the 2 temporal-channel model. Eccentricities range from 5° (*lightest markers*) to 40° (*darkest markers*). Marker size spans ± 1 SEM across 12 participants in each dimension and β weights were solved by fitting the 2 temporal-channel using data concatenated across Experiments 1 and 2.

REFERENCES

1.   Kaplan, E. & Benardete, E. The dynamics of primate retinal ganglion cells. *Prog Brain Res* **134**, 17-34 (2001).

2.   Hubel, D.H. & Wiesel, T.N. Laminar and columnar distribution of geniculo-cortical fibers in the macaque monkey. *J Comp Neurol* **146**, 421-450 (1972).

3.   Schiller, P.H. & Malpeli, J.G. Functional specificity of lateral geniculate nucleus laminae of the rhesus monkey. *J Neurophysiol* **41**, 788-797 (1978).

4.   Derrington, A.M. & Lennie, P. Spatial and temporal contrast sensitivities of neurones in lateral geniculate nucleus of macaque. *J Physiol* **357**, 219-240 (1984).

5.   Nassi, J.J. & Callaway, E.M. Parallel processing strategies of the primate visual system. *Nat Rev Neurosci* **10**, 360-372 (2009).

6.   Zeki, S. & Shipp, S. The functional logic of cortical connections. *Nature* **335**, 311-317 (1988).

7.   Maunsell, J.H., Nealey, T.A. & DePriest, D.D. Magnocellular and parvocellular contributions to responses in the middle temporal visual area (MT) of the macaque monkey. *J Neurosci* **10**, 3323-3334 (1990).

8.   Merigan, W.H. & Maunsell, J.H. How parallel are the primate visual pathways? *Annu Rev Neurosci* **16**, 369-402 (1993).

9.   Ferrera, V.P., Nealey, T.A. & Maunsell, J.H. Responses in macaque visual area V4 following inactivation of the parvocellular and magnocellular LGN pathways. *J Neurosci* **14**, 2080-2088 (1994).

10.   Van Essen, D.C. & Gallant, J.L. Neural mechanisms of form and motion processing in the primate visual system. *Neuron* **13**, 1-10 (1994).

11.   Shipp, S. & Zeki, S. Segregation of pathways leading from area V2 to areas V4 and V5 of macaque monkey visual cortex. *Nature* **315**, 322-325 (1985).

12.   Nassi, J.J., Lyon, D.C. & Callaway, E.M. The parvocellular LGN provides a robust disynaptic input to the visual motion area MT. *Neuron* **50**, 319-327 (2006).

13.   Seidemann, E., Poirson, A.B., Wandell, B.A. & Newsome, W.T. Color signals in area MT of the macaque monkey. *Neuron* **24**, 911-917 (1999).

14.   Brewer, A.A., Liu, J., Wade, A.R. & Wandell, B.A. Visual field maps and stimulus selectivity in human ventral occipital cortex. *Nat Neurosci* **8**, 1102-1109 (2005).

15.   Larsson, J. & Heeger, D.J. Two retinotopic visual areas in human lateral occipital cortex. *J Neurosci* **26**, 13128-13142 (2006).

16.   Singh, K.D., Smith, A.T. & Greenlee, M.W. Spatiotemporal frequency and direction sensitivities of human visual areas measured using fMRI. *Neuroimage* **12**, 550-564 (2000).

17.   Horiguchi, H., Nakadomari, S., Misaki, M. & Wandell, B.A. Two temporal channels in human V1 identified using fMRI. *Neuroimage* **47**, 273-280 (2009).

18.   Buxton, R.B., Wong, E.C. & Frank, L.R. Dynamics of blood flow and oxygenation changes during brain activation: the balloon model. *Magn Reson Med* **39**, 855-864 (1998).

19.   Boynton, G.M., Engel, S.A., Glover, G.H. & Heeger, D.J. Linear systems analysis of functional magnetic resonance imaging in human V1. *J Neurosci* **16**, 4207-4221 (1996).

20.   Boynton, G.M., Engel, S.A. & Heeger, D.J. Linear systems analysis of the fMRI signal. *Neuroimage* **62**, 975-984 (2012).

21.   Huettel, S.A. & McCarthy, G. Evidence for a refractory period in the hemodynamic response to visual stimuli as measured by MRI. *Neuroimage* **11**, 547-553 (2000).

22.   Ogawa, S.*, et al.* An approach to probe some neural systems interaction by functional MRI at neural time scale down to milliseconds. *Proc Natl Acad Sci U S A* **97**, 11026-11031 (2000).

23.   Birn, R.M., Saad, Z.S. & Bandettini, P.A. Spatial heterogeneity of the nonlinear dynamics in the FMRI BOLD response. *Neuroimage* **14**, 817-826 (2001).

24.   Mukamel, R., Harel, M., Hendler, T. & Malach, R. Enhanced temporal non-linearities in human object-related occipito-temporal cortex. *Cereb Cortex* **14**, 575-585 (2004).

25.   Friston, K.J., Frith, C.D., Turner, R. & Frackowiak, R.S. Characterizing evoked hemodynamics with fMRI. *Neuroimage* **2**, 157-165 (1995).

26.   Dumoulin, S.O. & Wandell, B.A. Population receptive field estimates in human visual cortex. *Neuroimage* **39**, 647-660 (2008).

27.   Kay, K.N., Naselaris, T., Prenger, R.J. & Gallant, J.L. Identifying natural images from human brain activity. *Nature* **452**, 352-355 (2008).

28.   Naselaris, T., Prenger, R.J., Kay, K.N., Oliver, M. & Gallant, J.L. Bayesian reconstruction of natural images from human brain activity. *Neuron* **63**, 902-915 (2009).

29.   Naselaris, T., Kay, K.N., Nishimoto, S. & Gallant, J.L. Encoding and decoding in fMRI. *Neuroimage* **56**, 400-410 (2011).

30.   De Valois, R.L. & Cottaris, N.P. Inputs to directionally selective simple cells in macaque striate cortex. *Proc Natl Acad Sci U S A* **95**, 14488-14493 (1998).

31.   De Valois, R.L., Cottaris, N.P., Mahon, L.E., Elfar, S.D. & Wilson, J.A. Spatial and temporal receptive fields of geniculate and cortical cells and directional selectivity. *Vision Res* **40**, 3685-3702 (2000).

32.   Conway, B.R. & Livingstone, M.S. Space-time maps and two-bar interactions of different classes of direction-selective cells in macaque V-1. *J Neurophysiol* **89**, 2726-2742 (2003).

33.   Kulikowski, J.J. & Tolhurst, D.J. Psychophysical evidence for sustained and transient detectors in human vision. *J Physiol* **232**, 149-162 (1973).

34.   McKee, S.P. & Taylor, D.G. Discrimination of time: comparison of foveal and peripheral sensitivity. *J Opt Soc Am A* **1**, 620-627 (1984).

35.   Watson, A.B. Temporal sensitivity. in *Handbook of Perception and Human Performance* (ed. K. Boff, L. Kaufman & J. Thomas) (Wiley, New York, 1986).

36.   Gawne, T.J. & Martin, J.M. Responses of primate visual cortical neurons to stimuli presented by flash, saccade, blink, and external darkening. *J Neurophysiol* **88**, 2178-2186 (2002).

37.   Sayres, R. & Grill-Spector, K. Relating retinotopic and object-selective responses in human lateral occipital cortex. *J Neurophysiol* **100**, 249-267 (2008).

38.   Weiner, K.S. & Grill-Spector, K. Not one extrastriate body area: using anatomical landmarks, hMT+, and visual field maps to parcellate limb-selective activations in human lateral occipitotemporal cortex. *Neuroimage* **56**, 2183-2199 (2011).

39.   Stigliani, A., Weiner, K.S. & Grill-Spector, K. Temporal Processing Capacity in High-Level Visual Cortex Is Domain Specific. *J Neurosci* **35**, 12412-12424 (2015).

40.   Gilaie-Dotan, S., Nir, Y. & Malach, R. Regionally-specific adaptation dynamics in human object areas. *Neuroimage* **39**, 1926-1937 (2008).

41.   Livingstone, M. & Hubel, D. Segregation of form, color, movement, and depth: anatomy, physiology, and perception. *Science* **240**, 740-749 (1988).

42. Gardner, J.L.*, et al.* Contrast adaptation and representation in human early visual cortex. *Neuron* **47**, 607-620 (2005).

43. Ungerleider, L.G. & Desimone, R. Projections to the superior temporal sulcus from the central and peripheral field representations of V1 and V2. *J Comp Neurol* **248**, 147-163 (1986).

44. Weiner, K.S.*, et al.* The Face-Processing Network Is Resilient to Focal Resection of Human Visual Cortex. *J Neurosci* **36**, 8425-8440 (2016).

45. Azzopardi, P., Jones, K.E. & Cowey, A. Uneven mapping of magnocellular and parvocellular projections from the lateral geniculate nucleus to the striate cortex in the macaque monkey. *Vision Res* **39**, 2179-2189 (1999).

46. Carrasco, M., McElree, B., Denisova, K. & Giordano, A.M. Speed of visual processing increases with eccentricity. *Nat Neurosci* **6**, 699-670 (2003).

47. Wager, T.D., Vazquez, A., Hernandez, L. & Noll, D.C. Accounting for nonlinear BOLD effects in fMRI: parameter estimates and a model for prediction in rapid event-related studies. *Neuroimage* **25**, 206-218 (2005).

48. Grill-Spector, K.*, et al.* Differential processing of objects under various viewing conditions in the human lateral occipital complex. *Neuron* **24**, 187-203 (1999).

49. Zhou, J., Benson, N.C., Kay, K. & Winawer, J. Temporal summation and adaptation in human visual cortex. *J Vis* **16**, 1228 (2016).

50. Kastner, S., De Weerd, P., Desimone, R. & Ungerleider, L.C. Mechanisms of directed attention in the human extrastriate cortex as revealed by functional MRI. *Science* **282**, 108-111 (1998).

ONLINE METHODS

Participants

Twelve participants (6 males, 6 females) with normal or corrected-to-normal vision participated in this study. All participants provided written informed consent, and the experimental protocol was approved by the Stanford University Institutional Review Board. Each individual participated in three fMRI sessions, two used to fit and validate the 2 temporal-channel model, and one session in which we conducted population receptive field (pRF) mapping[26] to define retinotopic cortical regions and another experiment to define human motion-sensitive area (hMT+)[51-53].

Temporal Channels Experiments

Visual stimuli

We used full-field phase-scrambled stimuli to generate robust visual responses while minimizing cognitive factors. Stimuli consisted of grayscale images that were generated by randomizing the phase spectrum of naturalistic images used in our previous publications[39] (**Fig. 1a**, *right*). We normalized the mean luminance and distribution of grayscale values in each image using the SHINE toolbox[54]. Stimuli were displayed to participants in the scanner using an Eiki LC-WUL100L projector (resolution: 1920 x 1200; refresh rate: 60 Hz) that was controlled by an Apple MacBook Pro using MATLAB (www.mathworks.com) and functions from Psychophysics Toolbox[55] (http://psychtoolbox.org). Participants viewed the projected images through an auxiliary mirror mounted on the RF coil. The mirror was adjusted in each participant such that stimuli spanned

approximately 40° of visual angle in the vertical dimension and 60° of visual angle in the horizontal dimension.

Experimental design

To obtain data that can be used to estimate and test the 2 temporal-channel encoding model, we introduce a novel fMRI paradigm that estimates independent sustained and transient contributions to fMRI responses across visual cortex using three experiments. All three experiments used the same stimuli, trial durations, and task, and only varied in their temporal presentation of the stimuli as detailed below and illustrated in **Fig. 1**.

Experiment 1 — largely sustained stimulation: phase-scrambled images were shown in trials of varying durations (2, 4, 8, 15, or 30 s per trial) in which a single phase-scrambled image was shown for the entire duration of the trial (**Fig. 1**, *blue*). Before and after each trial there was a 12 s baseline period (blank gray screen matched to the mean luminance of the stimuli). Across trials the number of stimuli (one per trial) and transients (at the onset and offset of each stimulus) are matched; just the duration of sustained stimulation varies. This experiment was designed to primarily activate the sustained channel, especially in the long trials.

Experiment 2 — largely transient stimulation: used the same trial durations and general experimental design as Experiment 1, except that in each trial 30 different phase-scrambled images were shown briefly, each for 33 ms. Thus, the number of stimuli, number of transients, and total duration of visual stimulation are matched across trial durations. The only factor that varied across trials was the inter-stimulus interval (ISI) between consecutively presented images. The ISI consisted of a blank mean-luminance screen that was 33 ms long in the 2 s trials, 100 ms in the 4 s trials, 233 ms in the 8 s trials, 467 ms in the 15 s trials, and 967 ms in the 30 s trials (**Fig.**

1, *red*). This experiment was designed to maximally drive the transient channel and minimally the sustained channel since each image was shown for only 33 ms.

Experiment 3 — combined sustained and transient stimulation: used the same design as Experiment 2, except that in each trial we presented 30 different phase-scrambled images in a continuous fashion without an ISI between sequential images. The durations of images (67, 133, 267, 500, or 1000 ms per image) varied across trials that were matched in length to Experiments 1, whereby the 67 ms presentations occurred in the 2 s trials and the 1000 ms presentations occurred in the 30 s trials (**Fig. 1**, *green*). This experiment was designed to drive both the sustained and transient channels: (i) during the entire trial duration there was always a stimulus on the screen and (ii) there were always 30 different images per trial.

Task: In all three experiments, participants were instructed to fixate on a small, central dot, and respond by button press when it changed color (occurring randomly once every 2–14 s, 8 s on average).

Experiments were designed such that if the sustained component is dominant, then Experiments 1 and 3 should yield similar responses since they have the same overall duration of stimulation. However, if the transient component is dominant then responses in Experiments 2 and 3 should be similar as they have the same number of transients. Finally, if transient and sustained channels contribute independently to responses, then fMRI signals in Experiment 3 that has both types of visual stimulation should be higher than either Experiments 1 or 2.

Data acquisition

Data were obtained with a TR of 1 s and a surface coil, collecting 16 slices per acquisition. To gain full coverage of occipitotemporal cortex, all participants completed two scan sessions on

different days with partially overlapping slice prescriptions. In each session participants viewed three 288 s runs of each experiment. Each run of each experiment contained of two repeats of each trial duration presented in random order. Data from different sessions were pooled in each participant's volume anatomy. The three runs of each experiment were blocked in each participant, and the order of experiments was counterbalanced between participants.

Population receptive field (pRF) mapping: To delineate retinotopic boundaries, we collected four 200 s runs of pRF mapping in each participant, same as in Dumoulin and Wandell[26]. In this experiment, a bar swept across a circular aperture (40° by 40° of visual angle) in eight directions and baseline periods were interspersed throughout each run. Participants performed the same color exchange fixation task as in the main experiments. We used the data to generate polar angle and eccentricity maps, which were used to define retinotopic visual areas as in our prior publications[38, 39, 56].

hMT+ localizer: To functionally define hMT+, in each participant we collected one 300 s run of a motion localizer experiment[38]. In this experiment, low contrast, 40° by 40°, concentric rings alternated between 16 s periods of motion (expansion/contraction) and 16 s periods of a stationary display. The experiment contained 6 cycles of alternating moving and stationary trials. Participants performed the color exchange fixation task.

Magnetic Resonance Imaging (MRI)

MRI data were collected using a 3T GE Signa MR750 scanner at the Center for Cognitive and Neurobiological Imaging (CNI) at Stanford University.

fMRI: We used a Nova 16-channel visual array coil (http://novamedical.com) to give participants a large unobstructed visual field of view. In each participant, we acquired two

partially-overlapping oblique slice prescriptions in separate scan sessions that together fully cover occipitotemporal cortex (resolution: 2.4 × 2.4 × 2.4 mm; one-shot T2*-sensitive gradient echo acquisition sequence: FOV = 192 mm, TE = 30 ms, TR = 1000 ms, and flip angle = 73°). We also collected T1-weighted inplane images with the same prescription as the functional data to align each participant's data to their high-resolution whole brain anatomy.

In a separate session, we obtained pRF mapping and hMT+ localizer data with the same RF coil setup and spatial resolution using 28 oblique slices covering the same brain volume but with a longer TR (resolution: 2.4 × 2.4 × 2.4 mm; one-shot T2*-sensitive gradient echo acquisition sequence: FOV = 192 mm, TE = 30 ms, TR = 2000 ms, and flip angle = 77°). We again collected T1-weighted inplane images in the same prescription to finely align inplane data to the whole brain anatomy of each participant.

Anatomical MRI: We acquired a whole-brain, anatomical volume in each participant using a Nova 32-channel head coil (resolution: 1 × 1 × 1 mm; T1-weighted BRAVO pulse sequence: TI = 450 ms, flip angle = 12°, 1 NEX, FOV = 240 mm).

Data analysis

Data were analyzed with MATLAB using code from vistasoft (http://github.com/vistalab) and FreeSurfer (http://freesurfer.net).

Data pre-processing

Functional data were aligned to each participant's native anatomical space using T1-weighted inplane images, and volumes acquired within the first 8 s of each run were discarded to allow time for magnetization to stabilize. We then performed slice time correction, motion

compensation (within and between scans), and transformed voxel time series to units of percent signal change. To normalize the baseline level of response across experiments, we subtracted from time points in each run the mean signal across the 4 s periods preceding the trial onsets in each run. This baseline removal procedure centers the mean response for the blank screen around zero to improve cross-validation performance[57] and to enable comparison of trial responses relative to the blank baseline.

Region of interest (ROI) definition

Areas V1, V2, V3, V3A, V3B, hV4, VO-1, VO-2, LO-1, and LO-2 were defined in each participant's native anatomical space using data from the pRF mapping experiment as in prior publications[38, 39, 56] (**Supplementary Fig. S2a**). To improve model performance in later visual areas, we fit one pRF to the run-averaged time series of each voxel using the compressive spatial summation (CSS) variant of the standard pRF model[58, 59]. ROIs were drawn bilaterally on each participant's cortical surface using the resulting polar angle and eccentricity maps. We excluded from ROI analyses voxels with pRF fits that explain less than 5% of their response variance. Dorsal visual areas V3A and V3B were also defined in each participant, but here we focus on regions in early visual cortex (V1, V2, and V3), ventral occipito-temporal cortex (hV4, VO-1, and VO-2), and lateral occipito-temporal cortex (LO-1, LO-2, and hMT+) because these regions have been more widely studied with regard to their temporal capacity than dorsal stream regions[7, 9, 24, 30-32, 60]. Data for V3A and V3B are included in **Supplementary Fig. S3**.

We defined hMT+ bilaterally in each participant using data from the motion localizer experiment as described in our previous publications[38]. hMT+ was defined as voxels in the

posterior inferior temporal sulcus[61] that responded significantly ($t > 3$) more to moving than stationary stimuli.

2 temporal-channel model

In typical analysis of fMRI responses[19, 25], the stimulus vector is convolved with the hemodynamic response function (HRF) to obtain a prediction of the fMRI response. However, this model does not account for distinct temporal channels of neural responses[30-32, 62]. To generate predicted fMRI responses accounting for the temporal channels, we implemented an encoding approach similar to Horiguchi[17].

The model illustrated in **Fig. 3** shows the procedure. First, we estimate the neural response of each channel by convolving the stimulus (**Fig. 3a**) separately with the neural impulse response function (IRF) for the sustained channel (**Fig. 3b**, *blue channel IRF*) and the transient channel (**Fig. 3b**, *red channel IRF*). This generates the predicted neural response to the visual stimulus for each channel. Then, the estimated neural responses for each channel are convolved with the hemodynamic response function (HRF, **Fig. 3c**) and summed to generate a prediction of the fMRI response. We use a general linear model (GLM) to solve for the contributions of the sustained and transient channels (β weights) given the measured fMRI responses.

The *sustained neural channel* is characterized by a monophasic IRF_S that generates a response for the entire duration of a stimulus. The *transient neural channel* is characterized by a biphasic IRF_T that generates a brief response at the onset and offset of an image[30-32, 34, 35]. The transient channel also contains a nonlinearity (squaring operation), that generates positive responses both from the onset and offset of the stimulus, as firing rates associated with transient 'on' or 'off' responses are positive[63] and metabolically demanding[17, 36]. The nonlinearities in this

model are at the neural level, and a linear relationship is assumed between the neural and BOLD responses.

Modeling the neural impulse response: Our model used impulse response functions estimated from human psychophysics[35] (**Fig. 3b**) to approximate the temporal sensitivity of the human visual system. These IRFs are expressed as the difference between excitatory and inhibitory linear filters. The excitatory filter is expressed as

$$h_1(t) = u(t) \cdot [\tau(n_1 - 1)!]^{-1} \cdot (t/\tau)^{n_1-1} \cdot e^{-t/\tau} ,$$

where $u(t)$ is the unit step function at time t; τ is a fitted time constant, and n_1 is the number of stages in the excitatory filter. The inhibitory filter incorporates the same time constant and is expressed as

$$h_2(t) = u(t) \cdot [\kappa\tau(n_2 - 1)!]^{-1} \cdot (t/\kappa\tau)^{n_2-1} \cdot e^{-t/\kappa\tau} ,$$

where κ is the ratio of time constants for the two filters and n_2 is the number of stages in the inhibitory filter. Both the sustained and transient channel IRFs are derived with the formula

$$h_c(t) = \xi[h_1(t) - \zeta h_2(t)] ,$$

where the normalization parameter ξ is used to match the height of the functions and is equal to 1 for IRF_S and 1.44 for IRF_T; the transience parameter ζ is equal to 0 for IRF_S and 1 for IRF_T. The other parameters are taken directly from Watson[35] and are: $\tau = 4.94$ ms, $\kappa = 1.33$, $n_1 = 9$, and $n_2 = 10$.

Modeling the visual input: Since the neural impulse response to a stimulus occurs on a millisecond timescale, we code each stimulus sequence in milliseconds. The stimulus is coded as a binary vector of ones and zeros, where one represents the presence of a stimulus and zero

indicates when there is no stimulus, just a blank mean luminance screen (**Fig. 3a**). To capture the digital transitions of the display (constrained by the 60 Hz refresh rate of the projector), a 17 ms gap is coded at the offset of each image. Next, the stimulus vector is convolved separately with each channel IRF to generate separate sustained and transient neural response predictors (**Fig. 3b**). To model the corresponding fMRI responses from each channel, each of the two neural response predictors are convolved with a HRF (**Fig. 3c**) that was sampled at the same high (millisecond) temporal resolution of the neural response predictors. Here, we slightly adapted the parameters of the canonical HRF implemented in SPM8 (www.fil.ion.ucl.ac.uk/spm/software/spm8) to better capture the rise and fall of the BOLD response in our measurements (delay of peak response = 5 s, delay of undershoot = 14 s, kernel length = 28 s).

Fitting the 2 temporal-channel model: Since the HRF acts as a low-pass temporal filter, this enables us to resample the predicted fMRI response to the lower temporal resolution of the acquired fMRI data (TR = 1 s). This resampled fMRI response predictor is compared to measured fMRI responses to solve for the contributions (β weights) of each channel. We normalized the predicted fMRI responses across the two channels, such that the maximal height is the same across both channels. Then we used a GLM to estimate the weights of the sustained (β_S) and transient (β_T) predictors by comparing the predicted responses to the measured response using data across all runs of Experiments 1 and 2. The GLM is applied to the mean response of each visual area in each participant. Quantification of model performance in each of Experiments 1 and 2 is presented in **Fig. 4d-e** for V1, in **Fig. 5c** for hV4 and hMT+, and in **Supplementary Fig.**

S2b-c for all ROIs. The predicted fMRI responses generated by the model are shown in **Fig. 4a** for V1 and **Supplementary Fig. S1** for other ROIs.

Validating the 2 temporal-channel encoding model: We assessed the predictive power of the 2 temporal-channel model by testing how well it predicts responses in independent data obtained in Experiment 3 (**Fig. 4b**). Thus, we coded the visual stimulation of Experiment 3 in the same manner described above, and convolved it separately with the IRFs of the sustained and transient neural channels to generate the neural predictors. These neural predictors were then convolved with HRF and downsampled to 1 s. Then we multiplied each channel's fMRI response predictor with its respective β weight (β_S or β_T) that was estimated with data concatenated across Experiments 1 and 2. We then tested how well the predicted responses matched the measured response in Experiment 3, operationalized as cross-validated R^2. That is, the proportion of response variance explained using β weights that were estimated from independent data. Although conceptually like the classical R^2 statistic, cross-validated R^2 can be negative when the residual variance of an inaccurate prediction exceeds the variance in the measured response. Quantification of cross-validation performance is shown in **Fig. 4f** for V1, in **Fig. 5c** for hV4 and hMT+, and in **Supplementary Fig. S2d** for all ROIs. The predicted fMRI responses generated by the model are shown in **Fig. 4b** for V1 and **Supplementary Fig. S1** for other ROIs.

Fitting and validating the standard model: For model comparison to the standard approach used in fMRI, we also fit a standard GLM to the data. The standard GLM predicts fMRI responses by convolving a stimulation vector with the HRF (basically steps **a** and **c** in **Fig. 3**). To describe the visual stimulation in our experiments, we used the same millisecond resolution visual stimulation vector as in the 2 temporal-channel model described above. After convolving

with the same HRF used in the 2 temporal-channel model, we downsampled the predicted

response to 1 s resolution to compare to measured fMRI responses. As the stimuli in all

experiments were identical and the only difference was the timing, we generated a single

predictor across Experiments 1 and 2 and fit one β weight. Like the 2 temporal-channel model,

we fit the standard model to data concatenated across all runs of Experiments 1 and 2, and we

then cross-validated this β weight on Experiment 3 data. Standard model predictions for V1 are

shown in **Fig. 2a** and for other ROIs in **Supplementary Fig. S1**. Model performance is quantified

separately for Experiments 1 and 2 in **Supplementary Fig. S2b-c**.

Model comparison: We used repeated measures analysis of variance (ANOVA) to

compare the performance of the 2 temporal-channel model to the standard model across the

visual hierarchy. To test for differences in the predictive power of the two models at various

stages, we performed a two-way repeated measures ANOVA with factors of model (2 temporal-

channel/standard) and visual field map cluster (early/ventral/lateral) on the cross-validated R^2

values from each ROI (see **Supplementary Fig. S2d** for ANOVAs including dorsal regions). For

the 2 temporal-channel model, we additionally tested for differences in the relative

contributions of the sustained and transient channels across the hierarchy using a two-way

repeated measures ANOVA with factors of temporal channel (sustained/transient) and visual

field map cluster (early/ventral/lateral) on the channel β weights estimated for each ROI using

data from Experiments 1 and 2 (**Fig. 6b**).

Noise ceiling calculation: To compare the level of noise in measurements from different

brain regions, we estimated the noise ceiling of each ROI using a procedure proposed by Kay[58].

This method estimates the maximal R^2 that a model could achieve given the level of noise in the

data by simulating noisy measurements of a signal (with noise characteristics matched to the data) and using a bootstrapping procedure to estimate the median accuracy with which any given model could explain the simulated measurements. This procedure was performed separately for the 2 temporal-channel model and the standard model, and we plot the average noise ceiling estimate across both models for each ROI in **Supplementary Fig. S2**.

Generating group parameter maps of temporal channel contributions: To map the topology of contributions from the transient and sustained channels across visual cortex, in each participant we fit the 2 temporal-channel model in each voxel using data from Experiments 1 and 2, as described above. We then generated in each participant's brain parameter maps of each temporal channel's β weights. To generate group maps, we first registered all participants' anatomy to the FreeSurfer average brain template using cortex-based alignment (CBA) in FreeSurfer version 5.3.c[64-67]. Then, we averaged these maps across participants on the common fsaverage cortical surface to obtain group maps (**Figs. 6a**, **7a**; **Supplementary Fig. S3b**). To independently validate our results from ROI analyses, group hV4, VO-1, VO-2, LO-1, LO-2, and hMT+ are outlined on the ventrolateral surface using the atlas developed by Wang and colleagues[68] (**Fig. 6b**, **Supplementary Fig. S3b**). Note that hMT+ is defined based on the union of TO-1 and TO-2 maps[53] from the Wang atlas[68]. To illustrate channel contributions in relation to the eccentricity map in early visual cortex, we used atlases developed by Benson and colleagues[69] to overlay the regional boundaries of V1, V2, and V3 and trace eccentricity bands on the group average (**Fig. 7a**).

Measuring temporal channel contributions across eccentricities: To quantify changes in the contributions of transient and sustained channels within regions in early visual cortex as a

function of eccentricity, we defined a series disc ROIs (each ~1 cm in diameter) in each

hemisphere of the fsaverage cortical surface using the tksurfer package included with FreeSurfer.

Using the Benson atlas[69], uniformly-sized ROIs were dilated around mesh vertices centered on

eccentricities of either 5°, 10°, 20°, or 40° (**see Fig. 7b**) both along the horizontal meridian

representations in V1 and along the ventral and dorsal borders of V2/V3. Note that: (i) we used

the Benson[69] atlas as it contains eccentricities further into the periphery that were not mapped

in pRF mapping experiment (visual angle was limited to 20° from fixation, see above), and (ii) we

placed disk ROIs along the horizontal meridian as the phase-scrambled stimuli used in

Experiments 1–3 extended further into the periphery in the horizontal than the vertical

dimension (30° vs. 20° degrees from fixation, respectively). The disc ROIs were then transformed

to each participant's native brain space, and we fit the two temporal-channel model to data from

Experiments 1 and 2 in each ROI as described previously (**Fig. 7b**). To compare differences in

temporal channel contributions across eccentricities between V1 and V2/V3, we used a three-

way, repeated measures ANOVA with factors of channel (transient or sustained), visual area (V1

or V2/V3), and eccentricity (5°, 10°, 20°, or 40°).

Explaining previously reported nonlinearities for short stimuli: To externally validate the 2

temporal-channel model, we simulated the temporal characteristics of visual stimulation in a

previous study by Birn et al.[23] that measured V1 responses to brief presentations of a

checkerboard stimulus that was contrast inverted at a rate of 8 Hz (see **Supplementary Fig. S4a**).

We used data from the Birn study because it showed other experimental conditions in which the

standard model underestimated measured fMRI responses using stimulus presentations in the

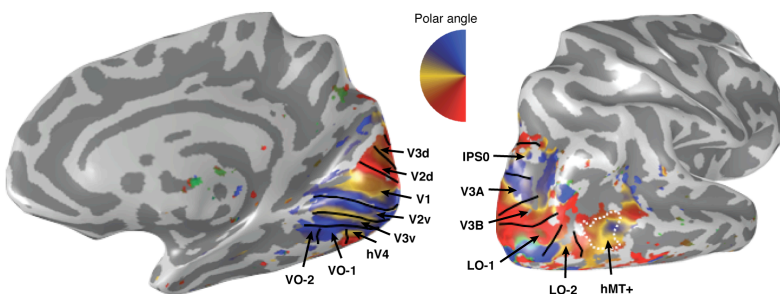millisecond range. To predict responses to this 8 Hz stimulus with our model, we coded each

125 ms phase of a flicker sequence as a separate image within a trial (as described for Experiment 3). Using this coding of the stimulus in the Birn study, we used our 2-temporal channel model to generate fMRI response predictors of each channel, and multiplied the predicted response of each channel using the β weights estimated for V1 across Experiments 1 and 2 (**Supplementary Fig. S4b**, *left*). Finally, we used the same stimulus model and the β weight estimated by the standard model for V1 (**Supplementary Fig. S4b**, *right*) to compare the validity of the two models.

SUPPLEMENTARY FIGURES
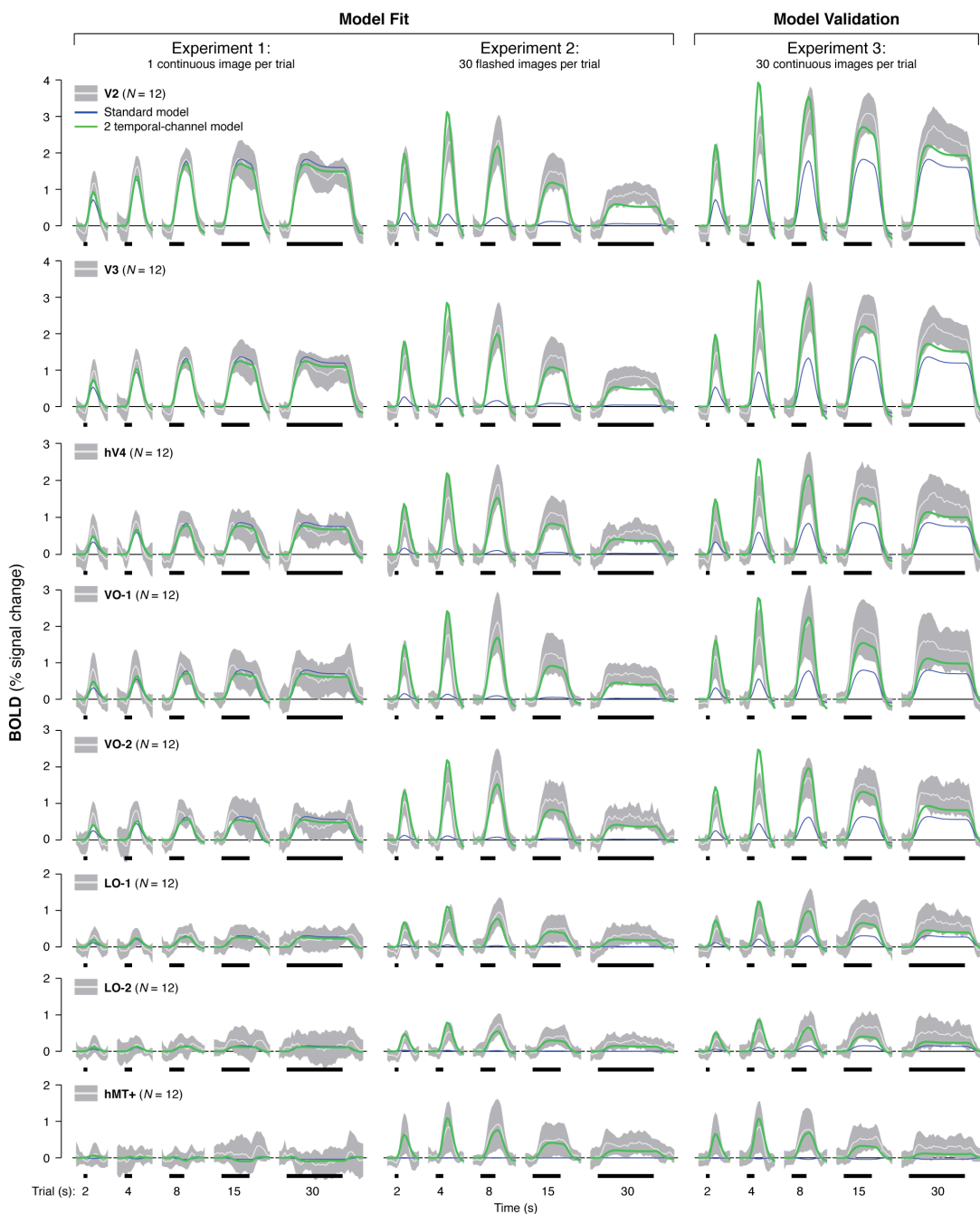
Supplementary Figure S1: Modeling sustained and transient contributions across the visual hierarchy. Each row depicts the average ROI response (*white*) ± 1 standard deviation (*gray*) across 12 participants. *Left:* Experiment 1; *Middle:* Experiment 2; *Right:* Experiment 3. Trial durations are indicated by the thick black lines below the x-axis, and curves extend 2 s before the onset and 12 s after the offset each trial. *Green:* predictions of the 2 temporal-channel model; *Blue:* predictions of the standard model. Both models are fit using data concatenated across Experiments 1 and 2 and then validated against data from Experiment 3.
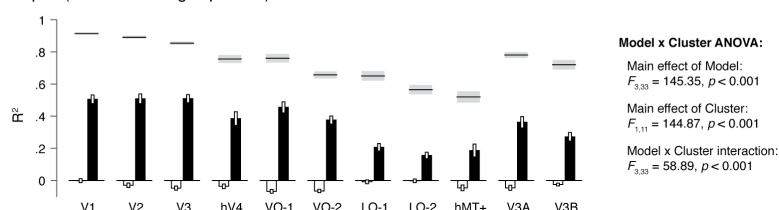
Supplementary Figure S2: Comparison of the variance explained by the 2 temporal-channel vs. standard model. (**a**) Definition of retinotopic visual areas in a representative participant. Boundaries of retinotopic areas (*black*) are overlaid on an example participant's inflated cortical surface depicting a polar angle map generated using pRF mapping. hMT+ is outlined with a dashed white line. (**b–d**) The performance of the 2 temporal-channel model and standard model is compared across four clusters of visual areas: *Early visual* (V1, V2, V3), *ventral* (hV4, VO-1, VO-2), *lateral* (LO-1, LO-2, hMT+), and *dorsal* (V3A, V3B). Both models are fit separately in each region using data concatenated across Experiments 1 and 2, and the accuracy (R^2) with which these β weights predict fMRI responses is quantified separately for (**b**) Experiment 1 and (**c**) Experiment 2. (**d**) Cross-validated R^2 of model predictions for independent data in Experiment 3. Note R^2 may be negative if the variance in the model prediction exceeds that of the data. *Error bars:* ± 1 SEM across 12 participants. *Black:* 2 temporal-channel model; *White:* standard model; *Gray line:* noise ceiling. Statistical significance of model fit comparison across visual areas was evaluated by a repeated-measures ANOVA for each experiment, shown beside each panel.
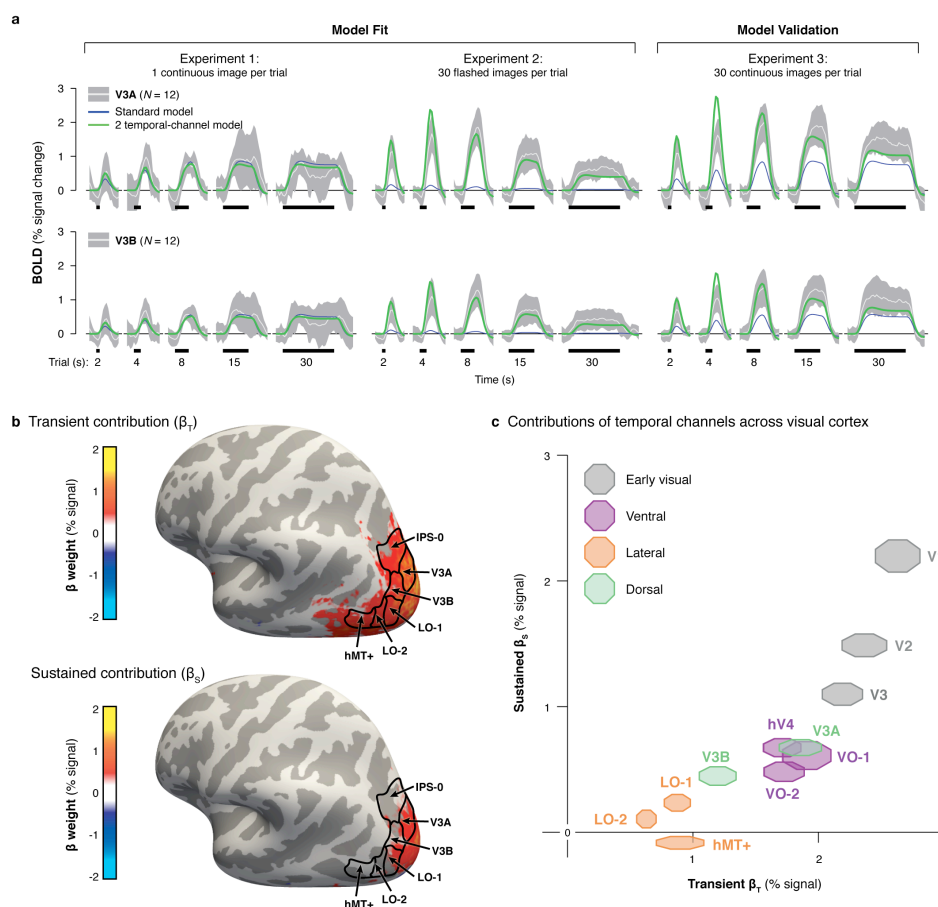
Supplementary Figure S3: Modeling sustained and transient contributions in dorsal retinotopic visual areas. (**a**) Each row depicts the average ROI response (*white*) ± 1 standard deviation (*gray*) across 12 participants for dorsal regions V3A and V3B. *Left:* Experiment 1; *Middle:* Experiment 2; *Right:* Experiment 3. Trial durations are indicated below the x-axis, and curves extend 2 s before the onset and 12 s after the offset each trial. *Green:* predictions of the 2 temporal-channel model; *Blue:* predictions of the standard model. Both models are fit using data concatenated across Experiments 1 and 2 and then validated against data from Experiment 3. (**b**) Group-averaged (*N* = 12) maps of the transient (*left*) and sustained (*right*) channels shown from a dorsolateral view. We first estimate β weights of each channel in each voxel in each participant's native brain space. β weight maps were transformed to the FreeSurfer average brain using cortex-based alignment and averaged across participants in this common cortical space. The resulting group maps were thresholded to exclude voxels with weak contributions ($-0.1 > \beta > 0.1$). Boundaries of dorsal and lateral regions (*black*) are derived from the Wang Atlas, with hMT+ as the union of TO-1 and TO-2. (**c**) The contributions of the transient (x-axis) and sustained (y-axis) channels to responses in each visual area as estimated by the 2 temporal-channel model. Marker size spans ± 1 SEM across 12 participants in each dimension and β weights were solved by fitting the 2 temporal-channel using data concatenated across Experiments 1 and 2.
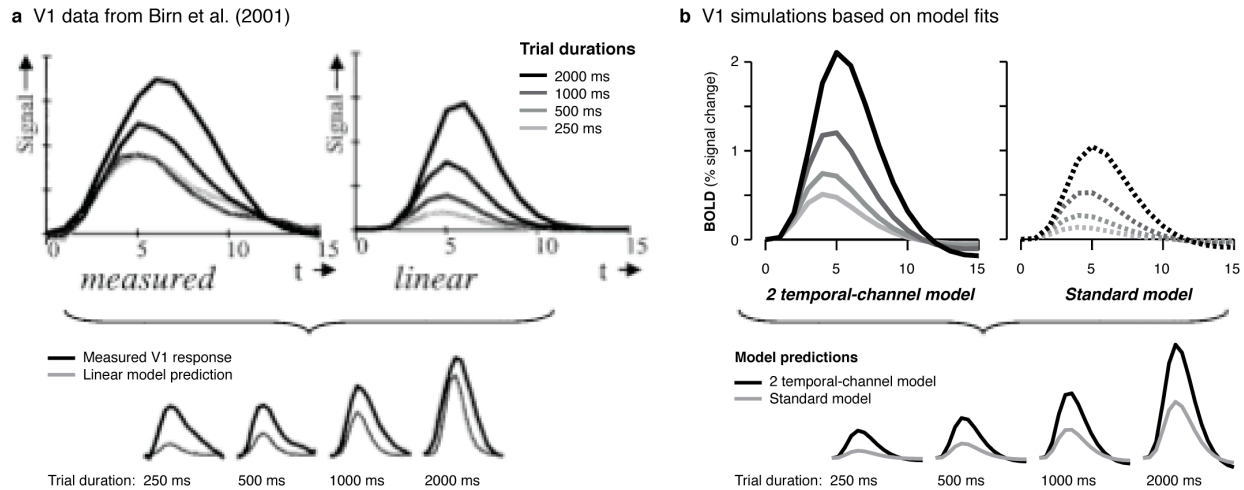
Supplementary Figure S4: The 2 temporal-channel model explains response nonlinearities for briefly presented stimuli. (**a**) Figure adapted from Birn et al. (y-axis values are unreported in original version). *Top left*: measured V1 responses to brief (250–2000 ms) presentations of a checkerboard stimulus that was contrast inverted at 8 Hz in all trial durations; *Top right*: predicted V1 responses based on a standard linear model solved using responses to longer presentations of the checkerboard stimulus. *Bottom*: same data as above except the measured and predicted fMRI responses are superimposed for each trial duration. (**b**) Simulated V1 responses to the stimuli used by Birn et al. that are derived with the β weights solved using models fit to V1 data from Experiments 1 and 2 of the present study. *Left*: predictions of the 2 temporal-channel model for each trial duration; *Right*: predictions of the standard model for each trial duration. *Bottom*: same data as above except the predictions of the two models are superimposed for each trial duration. The simulations show that the standard model replicates Birn et al.'s linear model and underestimate responses. In contrast, the 2 temporal-channel model better explains the measured responses (a-left) and predicts higher responses than the standard model in each duration (b-bottom).

ONLINE REFERENCES

51.   Tootell, R.B.*, et al.* Functional analysis of human MT and related visual cortical areas using magnetic resonance imaging. *J Neurosci* **15**, 3215-3230 (1995).

52.   Huk, A.C., Dougherty, R.F. & Heeger, D.J. Retinotopy and functional subdivision of human areas MT and MST. *J Neurosci* **22**, 7195-7205 (2002).

53.   Amano, K., Wandell, B.A. & Dumoulin, S.O. Visual field maps, population receptive field sizes, and visual field coverage in the human MT+ complex. *J Neurophysiol* **102**, 2704-2718 (2009).

54.   Willenbockel, V.*, et al.* Controlling low-level image properties: the SHINE toolbox. *Behav Res Methods* **42**, 671-684 (2010).

55.   Brainard, D.H. The Psychophysics Toolbox. *Spat Vis* **10**, 433-436 (1997).

56.   Weiner, K.S. & Grill-Spector, K. Neural representations of faces and limbs neighbor in human high-level visual cortex: evidence for a new organization principle. *Psychol Res* **77**, 74-97 (2013).

57.   Brouwer, G.J. & Heeger, D.J. Cross-orientation suppression in human visual cortex. *J Neurophysiol* **106**, 2108-2119 (2011).

58.   Kay, K.N., Winawer, J., Mezer, A. & Wandell, B.A. Compressive spatial summation in human visual cortex. *J Neurophysiol* **110**, 481-494 (2013).

59.   Kay, K.N., Weiner, K.S. & Grill-Spector, K. Attention reduces spatial uncertainty in human ventral temporal cortex. *Curr Biol* **25**, 595-600 (2015).

60.   McKeeff, T.J., Remus, D.A. & Tong, F. Temporal limitations in object processing across the human ventral visual pathway. *J Neurophysiol* **98**, 382-393 (2007).

61.   Dumoulin, S.O.*, et al.* A new anatomical landmark for reliable identification of human area V5/MT: a quantitative analysis of sulcal patterning. *Cereb Cortex* **10**, 454-463 (2000).

62.   Saul, A.B., Carras, P.L. & Humphrey, A.L. Temporal properties of inputs to direction-selective neurons in monkey V1. *J Neurophysiol* **94**, 282-294 (2005).

63.   Adelson, E.H. & Bergen, J.R. Spatiotemporal energy models for the perception of motion. *J Opt Soc Am A* **2**, 284-299 (1985).

64.   Fischl, B.*, et al.* Cortical folding patterns and predicting cytoarchitecture. *Cereb Cortex* **18**, 1973-1980 (2008).

65.   Hinds, O.*, et al.* Locating the functional and anatomical boundaries of human primary visual cortex. *Neuroimage* **46**, 915-922 (2009).

66.   Weiner, K.S.*, et al.* The Cytoarchitecture of Domain-specific Regions in Human High-level Visual Cortex. *Cereb Cortex* (2016).

67.   Fischl, B., Sereno, M.I., Tootell, R.B. & Dale, A.M. High-resolution intersubject averaging and a coordinate system for the cortical surface. *Hum Brain Mapp* **8**, 272-284 (1999).

68.   Wang, L., Mruczek, R.E., Arcaro, M.J. & Kastner, S. Probabilistic Maps of Visual Topography in Human Cortex. *Cereb Cortex* **25**, 3911-3931 (2015).

69.   Benson, N.C., Butt, O.H., Brainard, D.H. & Aguirre, G.K. Correction of distortion in flattened representations of the cortical surface allows prediction of V1-V3 functional organization from anatomy. *PLoS Comput Biol* **10**, e1003538 (2014).